ELSEVIER

Polymer 40 (1999) 4833–4843

polymer

# In situ formation of nanosized $TiO_2$ domains within poly(amide–imide) by a sol–gel process

Q. Hu, E. Marand*

*Department of Chemical Engineering, Virginia Polytechnic Institute and State University, Blacksburg, VA 24061 USA*

Received 30 July 1997; received in revised form 2 March 1998; accepted 23 March 1998

**Abstract**

Poly(amide–imide)/$TiO_2$ (PAI/$TiO_2$) composite films were prepared by an in situ sol–gel process. These composite films exhibited high optical transparency, having nanosized $TiO_2$ rich domains well dispersed within the PAI matrix. The size of the domains increased from 5 to 50 nm when the $TiO_2$ content was increased from 3.7 to 17.9% by weight. Hydrogen bonding interactions between the amide groups in the PAI and the hydroxyl groups on the inorganic oxide were observed. In comparison to the pure PAI polymer, the PAI/$TiO_2$ composite films exhibited higher glass transition temperature, an increase and flattening of the rubbery plateau modulus, and a decrease in crystallinity. 

*Keywords:* Sol–gel process; Poly(amide–imide)/$TiO_2$ composite films; Nanosized metal oxides

## 1. Introduction

In recent years much effort has been devoted to developing new materials created by modifying known polymers via the incorporation of a variety of inorganic additives by a sol–gel process. The resulting hybrid materials have had potential applications as abrasive-resistant coatings, catalysts, electronic and optical materials, and absorbents [1–9]. Hybrid organic–inorganic materials can be formed by reacting an inorganic alkoxide directly with an organic polymer or an oligomer having the appropriate functional groups, thus providing covalent linkages between the organic phase and the inorganic network [9–17]. In particular, polyimide–silica hybrid materials have been sucessfully prepared via this approach [13–17]. Alternatively, in situ polymerization of an alkoxide within a swollen polymer network can be used to form organic/inorganic composite materials without covalent crosslinks [18–26]. The size of the inorganic phase then depends upon the sol–gel conditions, the type of alkoxide, as well as on the nature of molecular interactions between the polymer and the inorganic oxide. High level of mixing can be achieved on a nano scale, particularly with polymers which contain functional groups such as carbonyls, hydroxyls or ether oxygens, which can form hydrogen bonds with the inorganic network [22–25]. This latter method is especially interesting because it can be employed to directly modify commercially available polymer systems.

The in situ formation of an inorganic network within a polymer matrix is governed by several parameters. The composite system is prepared by co-dissolving a precursor, a tetra-functional metal alkoxide with the polymer in a common solvent. A small amount of catalyst is added to catalyze the sol–gel reactions, which can be generalized into hydrolysis, alcoxolation, and oxolation [27,28] reactions. The sol–gel reactions of tetraethyltitanate (TET), for example, include the following reactions,

Hydrolysis

$$\equiv Ti(OEt)_4 + H_2O \rightarrow \equiv TiOH + EtOH;$$

Alcoxolation

$$\equiv Ti{-}OH + EtO{-}Ti\equiv \rightarrow \equiv Ti{-}O{-}Ti\equiv + EtOH;$$

Oxolation

$$\equiv Ti{-}OH + HO{-}Ti\equiv \rightarrow \equiv Ti{-}O{-}Ti\equiv + H_2O.$$

These reactions are concurrent and their relative rates are governed by pH, solvent, water to alkoxide ratio, concentration, type of catalyst and temperature [1,28]. In the case of polymer matrices, whose glass transition temperature is above ambient temperature, the final structure of the inorganic network and morphology of the composite is further influenced by the relative rates of vitrification and the rate of inorganic network formation [21]. In particular, pronounced differences in structure can occur, depending on whether the processing is carried out under acidic or basic conditions

* Corresponding author.

0032-3861/99/$ - see front matter 
PII: S0032-3861(98)00264-X

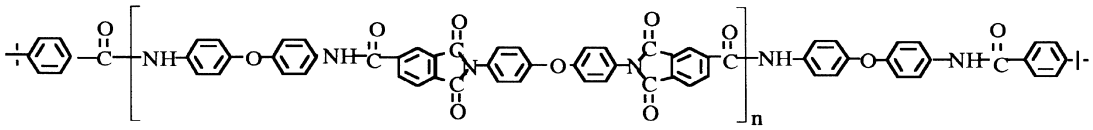

Fig. 1. Molecular structure of the poly(amide-imide) (PAI).

[1,27]. Based catalyzed systems with high water content, tend to consist of highly branched non-interpenetrating clusters, while acid catalyzed systems with low water content have linear or random branches. This structure results because under acidic conditions, the hydrolysis is faster than either of the two condensation reactions [1,27].

We are particularly interested in forming homogeneous polyimide/$TiO_2$ or polyimide/$SiO_2$ composites, which could ultimately be used for gas separation applications. As we wish to use the blend approach without covalent linkages between the organic and inorganic components, we have to rely on physical interactions to achieve a highly dispersed, homogeneous system. For this reason we had to incorporate an amide repeat unit into the polyimide structure, in order to facilitate hydrogen bonding with the inorganic component. Further, aromatic poly(amide–imide)s, (PAIs), combine superior mechanical properties, high thermal stability and chemical resistance [29,30] into one polymer. In the case of PAI/$TiO_2$ or PAI/$SiO_2$, we need to create highly dispersed, ceramic nanoclusters within the polymer matrix in order to achieve a high performance gas-separation membrane [31]. Because the point of zero charge (PZC) for $TiO_2$ metal oxide is at a higher pH (6.0) than that of $SiO_2$ (pH = 2.5), and the reaction kinetics of the Ti-based alkoxide are relatively fast, at low pH conditions there are many nucleating sites with highly positively charged surfaces, leading to repulsive forces between the $TiO_2$ particles [28]. This means that $TiO_2$ domains should be much smaller than $SiO_2$ domains formed under similar conditions. In fact, $SiO_2$ domains formed within PAIs and Torgamid by the sol–gel method are typically of the order of microns [32]. Hence, in order to satisfy our objectives, we have chosen to focus on the development and characterization of the PAI/$TiO_2$ composite system.

## 2. Experimental methods

### 2.1. Materials

The structure of the PAI used throughout this study is shown in Fig. 1. The PAI was synthesized from 4,4′-oxy(phenyl trimellitimide) (OPTMI)and 4,4′-oxydianiline (ODA) using *tert*-butyl benzoic acid (*t*-BBA) as the monofunctional endcapper [30]. The number average molecular weight, $M_n$, of the PAI as determined by GPC was $18.1 \times 10^3$. The polydispersity ratio $M_w/M_n$ was 2.7, where $M_w$ is the weight average molecular weight. The glass transition temperature of the PAI was 275°C [30].

Tetraethyltitanate (TET) was obtained from Aldrich Chemical Company. The titanium content of received TET was approximately 20% by weight. The TET was used as received without further purification. The content of the $Ti(OEt)_4$ was calculated assuming that all the titanium existed in the form of $Ti(OEt)_4$.

### 2.2. Fabrication of composite films

The Pyrex glass plate on which the polymer solution was cast was treated by an aqueous solution containing 2% KOH by weight for 24 h, and then washed by a sulfuric acid solution that contained ~ 5% of $K_2Cr_2O_7$ and 1% of water by weight. The plate was rinsed by double-distilled water and dried in an oven at ~ 120°C for 1–2 h and then cooled down to room temperature.

*N*,*N*-dimethyl acetamide (DMAC) solvent was used to dissolve the PAI. The incorporation of the $TiO_2$ network into the PAI was achieved by first dissolving approximately 0.5 g of the PAI in the DMAC solvent at a polymer concentration of 7% by weight. The TET sol was prepared by adding DMAC solvent, which contained a desired amount of HCl and double-distilled water, to TET under fast agitation. After being stirred for about 0.5–1 min, the TET sol was added immediately to the PAI solution under continuous agitation. An orbital shaker was used to eliminate any bubble formation. The solution was then stirred at ambient temperature for 30–36 h. The homogeneous transparent solution was then cast in a Teflon ring placed on the pretreated Pyrex glass plate at a controlled temperature. The drying rate was controlled by a heat lamp. The time of drying generally ranged from 12 to 48 h, depending on the desired drying rate. The drying was carried out in a closed box under dry nitrogen purge. After drying, the free standing films automatically lifted off. The film thickness achieved was on the order of 15–70 μm. Unless otherwise specified, the resulting films were cured in a vacuum at 100°C for 24 h, at 150°C for 12 h and finally at 200°C for 12 h. After curing, the residual DMAC and HCl in the film were extracted by immersing the film into ~ 300 ml methanol for 12–24 h, followed again by curing under vacuum at room temperature for 24 h, at 150°C for 24 h and at 220°C for another 24 h. Films treated in this way were analyzed by thermal gravimetric analysis (TGA) and were found to be free of solvents.

It should be pointed out that although we label the reacted inorganic component as $TiO_2$, the final product actually contains titanium-based domains possessing unreacted alkoxide groups, as well as hydroxyl groups, even after

Table 1
PAI/TET film fabrication and sample conditions

| No. | Film | $TiO_2$[a] (%by wt.) | $H_2O$/Ti (molar ratio) | Optical appearance |
|---|---|---|---|---|
| 1 | PAI/TET33/HCl(0.17)/CRm/FD | 5.3 | 7 | Transparent |
| 2 | PAI/TET50/HCl(0.17)/CRm/FD | 10.1 | 7 | Transparent |
| 3 | PAI/TET50/HCl(0.17)/CRm/SD | 10.1 | 7 | Opaque |
| 4 | PAI/TET50/HCl(0.11)/C70/FD | 10.1 | 7 | Transparent; gelled immediately |
| 5 | PAI/TET58/HCl(0.17)/CRm/FD | 13.4 | 5 | Transparent |
| 6 | PAI/TET58/HCl(0.17)/CRm/MD | 13.4 | 5 | Opaque |
| 7 | PAI/TET66/HCl(0.21)/CRm/FD | 17.9 | 6 | Transparent; brittle |

[a] Assuming 100% conversion of metal alkoxide to metal oxide.

heating to 200°C. Densification, i.e. complete condensation is not achieved until well above 700°C [1,27].

### 2.3. Characterization

Thermal gravimetric analysis (TGA) was carried out with a TG/DTA 200 Seiko I instrument. The heating rate of 10°C/min was used for all experiments. Prior to the experiments, a sample of 5–10 mg was put in an aluminum pan and preheated at 100°C in the TGA instrument for 5 min to remove any water absorbed from the atmosphere during the sample loading. The experiment was carried out in a nitrogen atmosphere.

Dynamic mechanical thermal analysis (DMTA) was carried out using a DMS 210 Seiko II instrument. The samples were cut to size, approximately 5 mm wide and 35 mm long. Experiments were carried out at 1 Hz at a heating rate of 2°C/min. The highest temperature reached was 450°C. The experiment was carried out in a nitrogen atmosphere. Samples treated under two different sets of conditions were examined. In the first stage, the samples were cured in a vacuum oven at 100°C for 24 h, then at 150°C for 24 h, followed by extraction by ethanol for 24 h. The samples were cured again in vacuum at room temperature for 24 h, then at 100°C for 24 h and finally at 150°C for 24 h. In the second stage, the same samples were subjected to an additional cure at 220°C in a vacuum for 24 h.

Wide angle X-ray diffraction (WAXD) analysis was carried out on a Nicolet diffractometer equipped with a STOE Bragg–Brentano type goniometer. CuKα radiation of the wavelength 1.54 Å was used after monochromatization through a graphite monochromator. Data was collected from 5 to 50° with 0.05° increments.

Transmission electron microscopy (TEM) analysis was performed on thin cross-sections 800–1200 Å thick, using a Phillips EM-420 scanning transmission electron microscope (STEM) operated in the transmission mode at 100 kV. The samples for the TEM analysis were microtomed at ambient temperature to obtain the cross-section through the thickness of sample.

Infrared transmission spectra were obtained using a Fourier transform infrared (FTIR) spectrometer, BIO-RAD FTS-40A from Bio-rad Digilab Corporation. The spectral resolution was 4 $cm^{-1}$. Samples were prepared by directly casting the solution onto KBr discs at room temperature. The cast solution was heated under a heat lamp for about 10 min to drive off the majority of the DMAC solvent. Subsequent treatments are outlined in the results section, as they varied. The sample temperature was controlled with a CN2011 Programmable Temperature Controller manufactured by Omega Technologies. The temperature sensor was a J-type iron vs. copper–nickel thermocouple, and the maximum error was ± 2°C.

## 3. Results and discussion

### 3.1. Film appearance

Optical transparency can be often used as an initial criterion for the homogeneous mixing of organic and inorganic components. When the inorganic domains and the polymer matrix have different refractive indices, an optically opaque film should typically contain iorganic domains larger than 200 nm. This is generally the lower bound detected by light scattering methods [33]. In contrast, the scattering effect of light becomes negligible if the inorganic domains are appreciably smaller than 200 nm, giving rise to an optically transparent film. The optical appearance of some PAI/$TiO_2$ composite films, along with the fabrication conditions, are given in Table 1.

The nomenclature adopted to describe the fabrication conditions of each composite includes five parts. For example, PAI/TET50/HCl(0.17)/C70/FD includes the following information in series: polymer name/mol percent of the metal alkoxide with respect to the amide–imide repeat unit in the PAI; TET(50) = 50% TET by mole/catalyst concentration; HCl(0.17) = 0.17 mole HCl per liter of solvent/casting temperature; C70 = 70°C, CRm = room temperature/drying rate; SD = slow drying, approximately 90% of solvent was evaporated within 48–72 h; FD = fast drying, 90% of solvent was evaporated within 8–12 h;

Table 2
The $TiO_2$ content as determined by TGA at 750°C in air atmosphere

| | Sample no. in Table 1 (film) | | |
|---|---|---|---|
| | 1 (PAI/$TiO_2$ 5.3%) | 2 (PAI/$TiO_2$ 10.1%) | 7 (PAI/$TiO_2$ 17.9%) |
| Theoretical % $TiO_2$ by wt. | 5.3 | 10.1 | 17.9 |
| Measured % $TiO_2$ by wt. | 3.7 | 8.8 | 16.1 |
| Loss of $TiO_2$ | 1.6 | 1.3 | 1.8 |
| % $TiO_2$ incorporated | 69.8 | 87.1 | 88.8 |

MD = moderate drying, 90% of solvent was evaporated within 12–48 h.

The optical appearance of films summarized in Table 1 suggests that the PAI/$TiO_2$ composite films can be transparent if the fabrication conditions are correctly selected. The PAI–TET solution of sample 4 in Table 1, gelled immediately at a low HCl concentration and high casting temperature, leading to an optically transparent composite film, although after drying many voids were visible. Thus, fast drying at an elevated temperature leads to microvoid formation, as the polymer chains do not have time to relax. Further, the attraction among the $TiO_2$ particles is enhanced at low HCl concentrations as compared to high HCl concentrations because a higher pH value is closer to the PZC at pH = 6.0 for $TiO_2$. As a consequence, further condensation of the Ti ethoxide and hydroxide units, as well as possibly molecular interactions of the inorganic components with the PAI chains reduce the mobility of whole system. This phenomenon is not expected to occur at relatively high HCl concentrations because the $TiO_2$ particles at low pH are positively charged and repel each other.

Slow drying is another unfavorable condition for the fabrication of transparent composite films as demonstrated by samples 3 and 6, shown in Table 1. The slow drying extends the time for the solution to maintain a relatively low viscosity, and hence the particles can move more freely in a long period of time as compared to the fast drying. This increases the possibility for the particles to collide with each other and to continue to grow. In principle, coagulation of the particles should be reduced if they can form hydrogen bonds with the PAI component, thus introducing an additional constraint on the movement of the particles.

### *3.2. TGA study of $TiO_2$ content within the PAI*

The actual content of the $TiO_2$ in the PAI/$TiO_2$ composites can be determined from TGA analysis. As most polymers are essentially pyrolyzed before reaching 600°C in an air atmosphere, while $TiO_2$ remains thermally stable over 1000°C in an air atmosphere, the remaining residue should reflect the actual $TiO_2$ content. The $TiO_2$ content of the PAI/$TiO_2$ composites was analyzed by TGA and is presented in

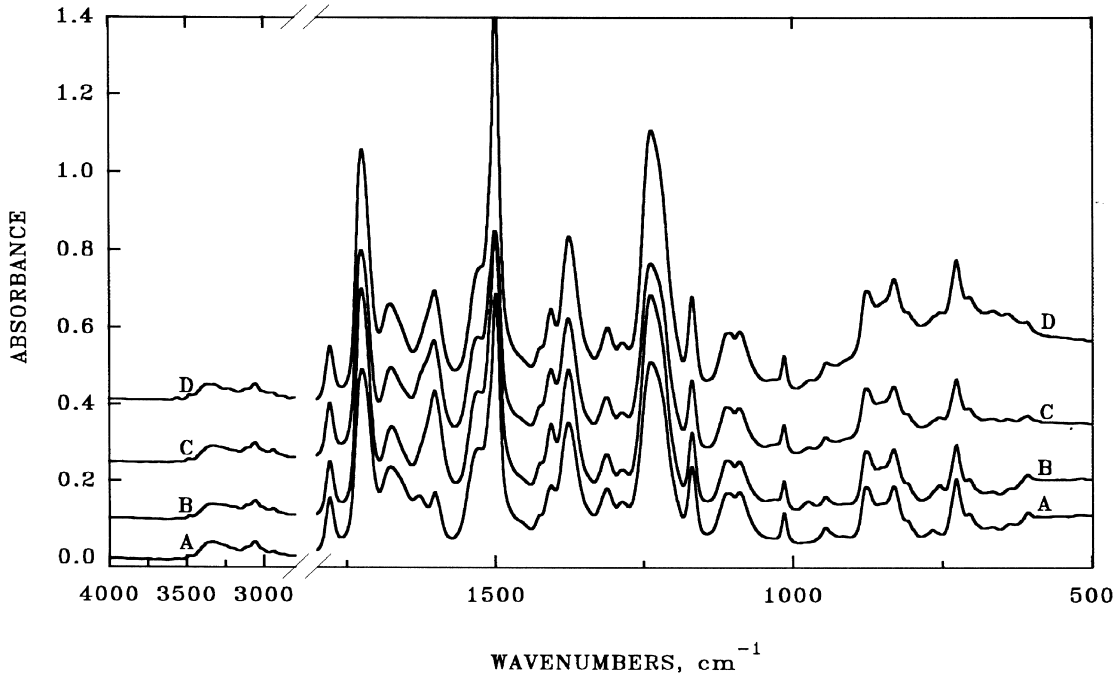


Fig. 2. FTIR spectra of the unfilled PAI and the PAI/$TiO_2$ composites at 100°C. (A) PAI; (B) PAI/$TiO_2$ (5.3%); (C) PAI/$TiO_2$ (10.1%); (D) PAI/$TiO_2$ (17.9%).

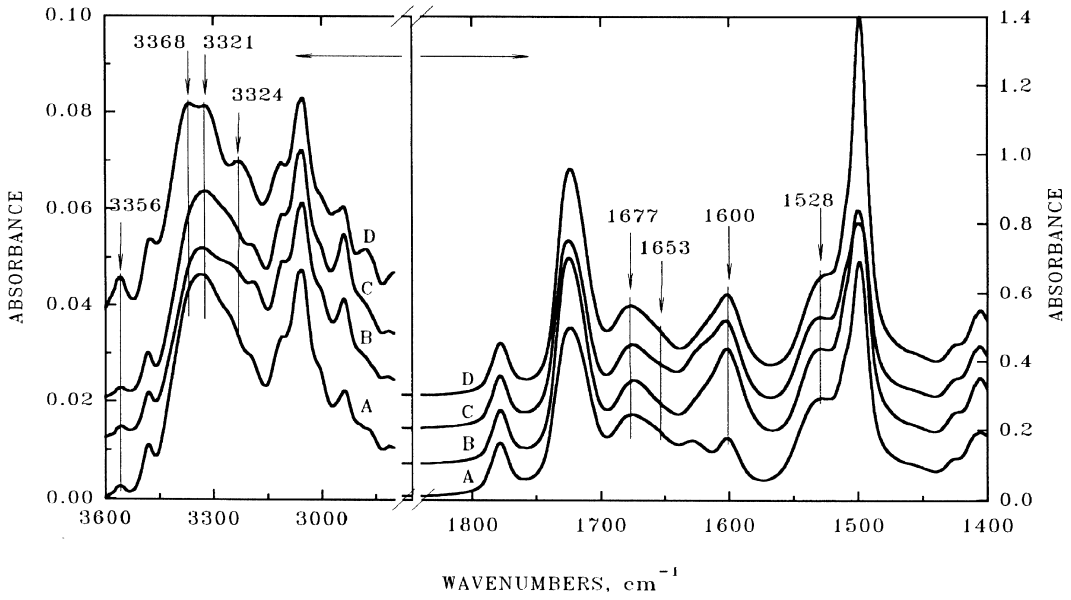


Fig. 3. FTIR spectra of the pure PAI and the PAI/$TiO_2$ composites at 100°C. (A) PAI; (B) PAI/$TiO_2$ (5.3%); (C) PAI/$TiO_2$ (10.1%); (D) PAI/$TiO_2$ (17.9%).

Table 2. All the samples shown in Table 2 were found by TGA to be solvent free [32]. The causes for the low percentage of incorporation of the PAI/$TiO_2$ (5.3%) composite are unknown, however some loss may arise during the methanol extraction process. It has been reported, for example, that treatment with methanol completely washes out the palladium salt incorporated within a 12F-poly(amide–imide) [29].

### *3.3. FTIR studies of the interaction between the PAI and $TiO_2$*

The general features of the FTIR spectra of the pure PAI polymer and the PAI/$TiO_2$ composites with different $TiO_2$ contents are shown in Fig. 2. The spectra in Fig. 2, and all the spectra throughout this article, have been normalized based on the intensity of the imide C=O stretch near 1780 cm$^{-1}$, as the change in the intensity of this band due to molecular interactions is negligible.

$TiO_2$ has a broad and strong absorption band from approximately 800 to 450 cm$^{-1}$ [34,35]. Accordingly, as shown in Fig. 2, the intensity of this region increases with increasing $TiO_2$ content. The discussion presented in the following text will be focused on the N–H and the amide C=O regions as these two regions contain the most important information on the interactions between the $TiO_2$ and the PAI components. The carbonyl region consists of two types of carbonyl groups; the amide C=O group in the PAI polymer, denoted here as amide C=O and the C=O group of the DMAC solvent, denoted here as DMAC C=O. For sake of clarity, the N–H and the amide C=O regions at 100°C in Fig. 2 are replotted as shown in Fig. 3. The thin film samples used in the infrared transmission studies reflect the physical state of the organic–inorganic system at the latter stages of film formation, as these samples are not yet fully cured and solvent exchange has not been carried out. The unfilled PAI, as shown in curve A, contains DMAC solvent but no water. The DMAC solvent has a well-defined frequency at 1646 cm$^{-1}$ due to the free DMAC C=O stretch [36]. Accordingly, the band appearing at 1630 cm$^{-1}$, which is 16 cm$^{-1}$ lower than 1646 cm$^{-1}$, suggests that the DMAC C=O groups function as proton acceptors and form hydrogen bonds with the N–H groups in the PAI. Upon incorporating $TiO_2$ into the PAI, the band at 1600 cm$^{-1}$, associated with O–H bending of monomeric water [37,38], increases in intensity. Although the O–H bending mode of the monomeric water at 1600 cm$^{-1}$ overlaps with the characteristic band of the benzene ring [36], the higher intensity of this band in the PAI/$TiO_2$ composite, in comparison to the unfilled PAI, clearly shows the existence of water in the composite system. This is not surprising, because water is not only added to the system, but is also a product of one of the condensation reactions. The free amide C=O band centered at 1677 cm$^{-1}$ and the hydrogen-bonded amide C=O band at 1653 cm$^{-1}$ are not affected by the incorporation of the $TiO_2$ component. Basically, all spectra of the PAI/$TiO_2$ composites, as shown in curves B, C and D in Fig. 3, do not show the evidence of hydrogen bonding between the amide C = O and the $TiO_2$ at this stage of the film processing.

However, a significant change in the N–H region, as shown in Fig. 3, is clearly visible. An increase in the $TiO_2$ content to 17.9% causes the N–H stretch to split evidently into two bands. One band is the free N–H at 3368 cm$^{-1}$ and another is the hydrogen bonded N–H at 3321 cm$^{-1}$. The intensity of the hydrogen-bonded N–H at 3321 cm$^{-1}$ increases clearly with the increase in the $TiO_2$ content. The dependence of the hydrogen-bonded N–H groups on

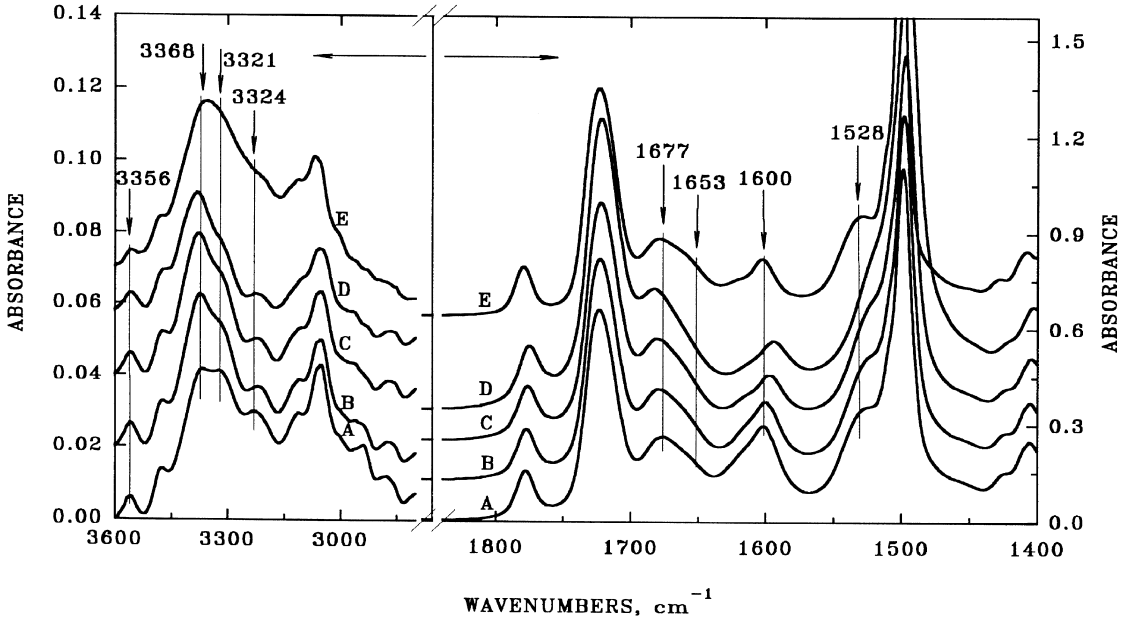


Fig. 4. FTIR spectra of the PAI/$TiO_2$ (17.9%) composite at varying temperatures. (A) 100°C; (B) 150°C; (C) 200°C; (D) 260°C; and (E) 35°C.

the $TiO_2$ content and thereby on the number of the Ti–OH groups, suggests that there is a hydrogen bonding interaction between the N–H and the Ti–OH or Ti–$OCH_2CH_3$ groups.

As mentioned earlier, all the composites films at this stage also contain water and the hydrogen bonded DMAC solvent. The water and solvent, as well as the self hydrogen bonding between the amide C=O and N–H in the PAI, may also cause a significant increase of intensity in the hydrogen bonded N–H band. Further confirmation of the hydrogen bonding interaction between the N–H and the Ti–OH was made with the aid of temperature experiments.

The spectra of the PAI/$TiO_2$ (17.9%) composite at different temperatures are shown in Fig. 4. The intensities near 1600 cm$^{-1}$, associated with the DMAC solvent and water, decrease appreciably as the temperature is increased from 100 to 200°C as shown in curves A, B and C. However the change becomes insignificant when the temperature increases further from 200 to 260°C, suggesting that the solvents have been removed. Also, the amide C=O region shows no appreciable evidence of hydrogen bonded amide C=O, as demonstrated by curves A through D in Fig. 4. This indicates that very little self-hydrogen bonding exists between the amide C=O and N–H in the PAI over the entire temperature range examined. In contrast, the 3321 cm$^{-1}$ band, characteristic of hydrogen-bonded N–H groups, decreases with increasing temperature, again reflecting the decrease of water and DMAC solvent in the system.

As the DMAC solvent was removed by the time the sample reached 260°C, subsequent sample E in Fig. 4 collected at 35°C should reflect hydrogen bonding interactions in the PAI/$TiO_2$ (17.9%) composite without the effect of solvents. Indeed, cooling to 35°C causes the N–H band at 3321 cm$^{-1}$ to become broad and to shift to lower wavenumbers, indicating an increase in the number of hydrogen-bonded N–H groups. As, there is virtually no corresponding change in the carbonyl region, we conclude that this is a result of hydrogen bonding between the N–H groups in the polymer and Ti–OH groups in the inorganic domains.

One would expect that the relative strengths of the hydrogen bonding interaction between the polymer and the inorganic component compared to the hydrogen bonding within the polymer itself, should affect the morphology of the system.

### *3.4. Morphology of the pure PAI polymer and the PAI/$TiO_2$ composites*

Transmission electron microscopy was used to study the difference in the morphology of the composites. The TEM micrographs of the PAI with varying $TiO_2$ contents are illustrated in Fig. 5. The dark portions represent the electron denser $TiO_2$ phase. The phase contrast, as shown in Fig. 5(A) for the pure PAI polymer, can be observed because the magnification is 400 000. In our discussion of the morphologies of the PAI/$TiO_2$ composites, the term domain is understood as a collection or an aggregate of metal oxide particles, which, as mentioned before, can also contain unreacted functional groups, such as the alkoxide group –$OC_2H_5$ and the hydroxyl group –OH. Judging by the appearance in the TEM micrographs, the aggregation of the $TiO_2$ particles in the PAI/$TiO_2$ (5.3%) composite is weak and the maximum size of the $TiO_2$ domains is less than 5 nm. The number in the brackets is the $TiO_2$ content by weight, based on 100% conversion from TET to $TiO_2$. An increase in the $TiO_2$ content to 10.1% and to 17.9%, as shown in Fig. 5(C)

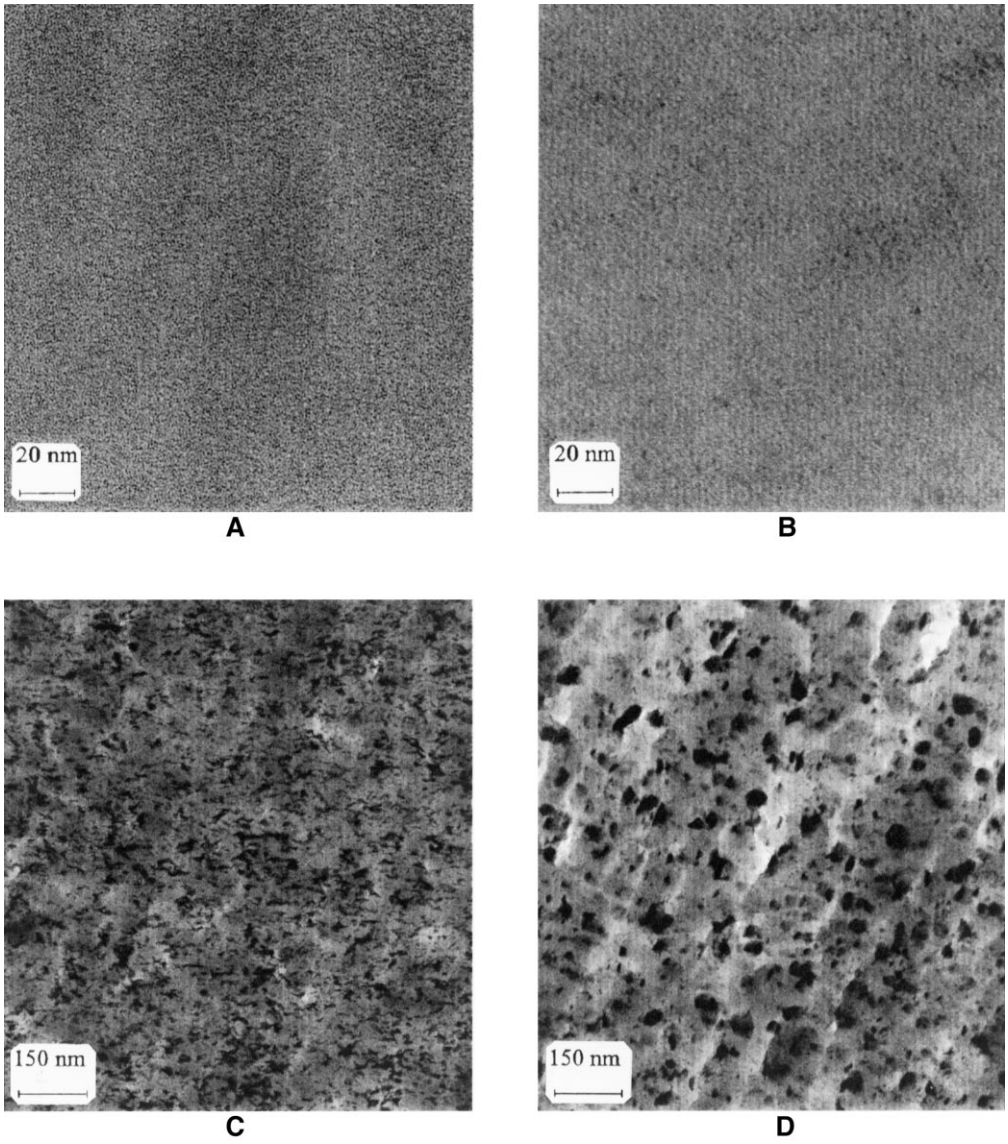


Fig. 5. Transmission Electron Micrographs of the pure PAI and the PAI/$TiO_2$ composites. (A) PAI; (B) PAI/$TiO_2$ (5.3%); (C) PAI/$TiO_2$ (10.1%); and (D) PAI/$TiO_2$ (17.9%).

and (D), leads to a larger $TiO_2$ domain size. In the PAI/$TiO_2$ (10.1%) composite, the majority of the $TiO_2$ domains have an average diameter of 30 nm or less. The domains have a loose, interconnected structure, as opposed to the discrete $TiO_2$ domains found in the PAI/$TiO_2$ (17.9%) composite. Fig. 5(D) shows that the $TiO_2$ domains have a distribution of sizes, all below 50 nm. The FTIR studies discussed previously have demonstrated that hydrogen bonding interactions exist between the $TiO_2$ particles and the amide component in the PAI polymer. These interactions are also believed to be partially responsible for the formation of the nanosized $TiO_2$ domains within the PAI matrix and the relatively high level of mixing between the two components. What is interesting is that the $TiO_2$ domain size also increases with increasing $TiO_2$ content. This suggests that, in addition to hydrogen bonding interaction between the polymer and the $TiO_2$ particles, which enhance the miscibility of the organic–inorganic system, there also exist attractive interactions between the particles themselves, which cause them to aggregate. Such effects may in fact be competitive.

### *3.5. The effect of $TiO_2$ domains on the dynamic mechanical properties of the PAI*

The smaller the $TiO_2$ domains, the larger the surface area which permits interfacial interactions between the $TiO_2$ and the PAI. Such interfacial interaction should have an effect on the thermal and mechanical properties of the polyamide-imide. The DMTA results of the composites with a $TiO_2$ content of 5.3% and 10.1% along with the pure PAI polymer are given in Fig. 6. The PAI/$TiO_2$ (17.9%) composite was

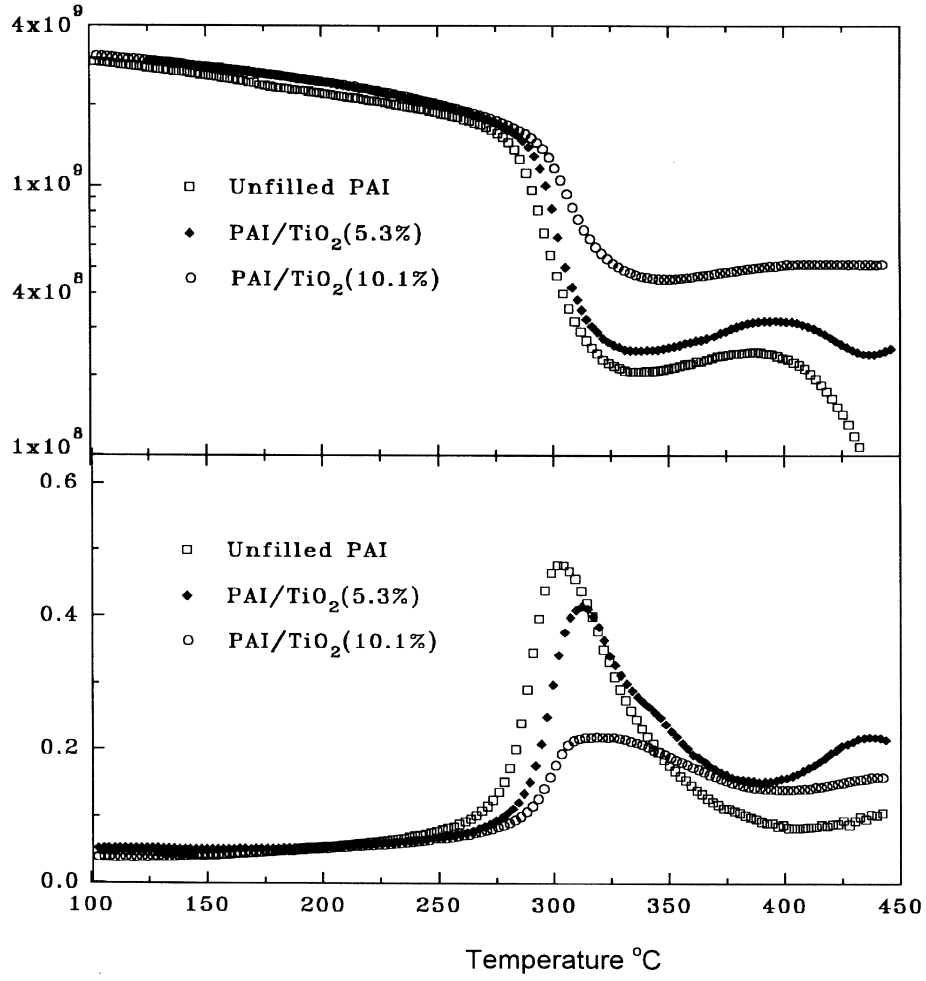


Fig. 6. The DMTA of the pure PAI polymer and the PAI/$TiO_2$ composites, cured at 150°C.

too brittle for DMTA analysis. The storage moduli before the glass transition ( ~ 275°C) are essentially the same for all the samples. In the case of the pure PAI polymer, the storage modulus drops from approximately $2 \times 10^9$ Pa at 270°C at the onset of the glass region to about $2 \times 10^8$ Pa at 330°C. In the rubbery region, a drop of only one decade is far less than the three decades for a typical amorphous glassy polymer [39]. However, interestingly, the modulus increases slightly in the region from 330 to 390°C. Because, a related study of this same polymer showed a significant crystallinity after the sample was annealed at 325°C for 3 min [30], and given the slow heating rate of 2°C/min in our own experiments, it is possible that the rise in the observed modulus is a result of a crystallization process. The modulus begins to drop after 390°C due to viscous flow of the amorphous PAI and the melting process of the crystallites. Whether or not crystallinity exists in the PAI before passing through the glass transition will be examined by WAXD measurements.

As shown in Fig. 6, the dip in the modulus centered at 330°C decreases with increasing the $TiO_2$ content. This suggests that the incorporated $TiO_2$ domains reduce the segmental mobility and thereby make the crystallization of the PAI more difficult. Further, the rubbery plateau modulus increases with increasing the $TiO_2$ content. In the case of the PAI/$TiO_2$ (10.1%) composite, the modulus in the rubbery region levels off after approximately 350°C, which is a typical response of a crosslinked elastomer, suggesting that the $TiO_2$ domains function as physical crosslinks. In addition to the modulus changes, there is a significant shift in the loss tangent peak to higher temperatures with increasing $TiO_2$ content, again reflecting reduced segmental mobility. The glass transition temperature shifts from 300°C in the pure PAI, to 312°C in the PAI/$TiO_2$ (5.3%) composite, and to 318°C in the PAI/$TiO_2$ (10.1%) composite. The loss tangent peak also decreases and broadens with increasing $TiO_2$ content, reflecting an increase in heterogeneity of the molecular motions of the PAI chains.

Post-curing at a elevated temperature also leads to a change in the dynamic mechanical properties, particularly in the case of the PAI/$TiO_2$ (10.1%) composite film, whose plateau modulus actually increases with temperature. The samples shown in Fig. 7 were subjected to additional cure at 220°C in a vacuum for 24 h after the sample treatment given

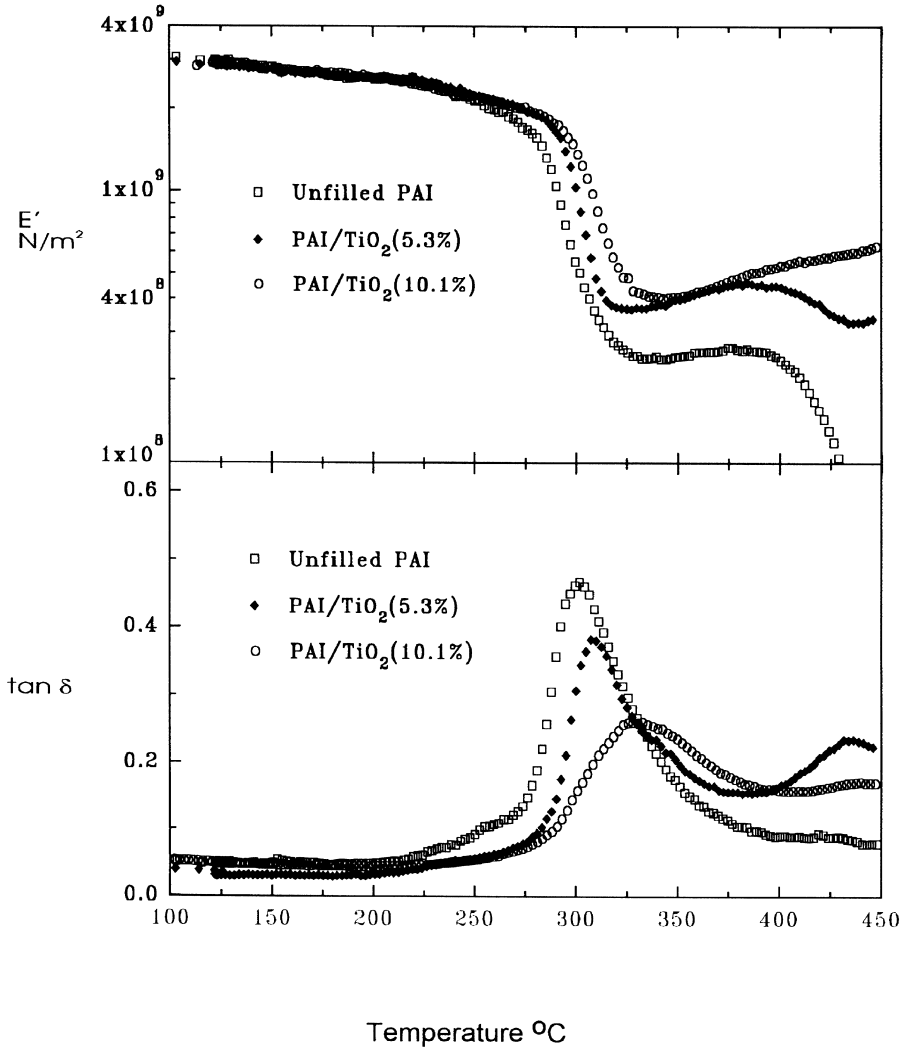


Fig. 7. DMTA of pure PAI polymer and PAI/$TiO_2$ composites. Post-cured samples at 220°C.

in Fig. 6. Annealing at this temperature drives the condensation reactions of the Ti–OH or unhydrolyzed alkoxide groups, forming water and other by-products. The loss of these groups is unavoidably accompanied by a contraction of the $TiO_2$ domains [1,27]. As a result, parts of polymer chains trapped in these domains become strained and experience reduced segmental mobility. In the dynamic mechanical properties, this change is reflected by an increase in the plateau modulus and a shift of the loss tangent to higher temperatures.

### *3.6. The effect of the $TiO_2$ domains on the crystallization of the PAI*

While there is evidence that PAI crystallizes at 325°C [30], whether or not any crystallinity is induced during the fabrication process of the sample films can be determined from WAXD measurements. The WAXD patterns of the PAI/$TiO_2$ composites along with the pure PAI polymer are shown in Fig. 8. The highest cure temperature for all the samples is 220°C, much lower than the glass transition temperature of $\sim$275°C and the crystallization temperature of $\sim$325°C of the pure PAI polymer. The WAXD patterns of the PAI/$TiO_2$ composites, shown by curves B and C reveal essentially an amorphous halo, similar in shape to the WAXD pattern of the amorphous PAI polymer. As $TiO_2$ exists in an amorphous state and still contains unreacted alkoxide and hydroxyl groups, none of the typical crystalline peaks, associated with the pure $TiO_2$ anatase and rutile forms [34,40] can be discerned. The decrease in scattering intensity with increasing $TiO_2$ content most likely results from the absorption of radiation by the inorganic component. While the shapes of the amorphous halo are the same in all three WAXD patterns, the pure PAI polymer, nevertheless, exhibits a small peak centered at 19°, that is not evident in the composite samples. A WAXD study by Sekharipuram has observed a sharp peak centered at 20° in the WAXD pattern of the pure PAI polymer annealed at 325°C for only 3 min. This suggests that the pure PAI may experience some solvent-induced crystallization during

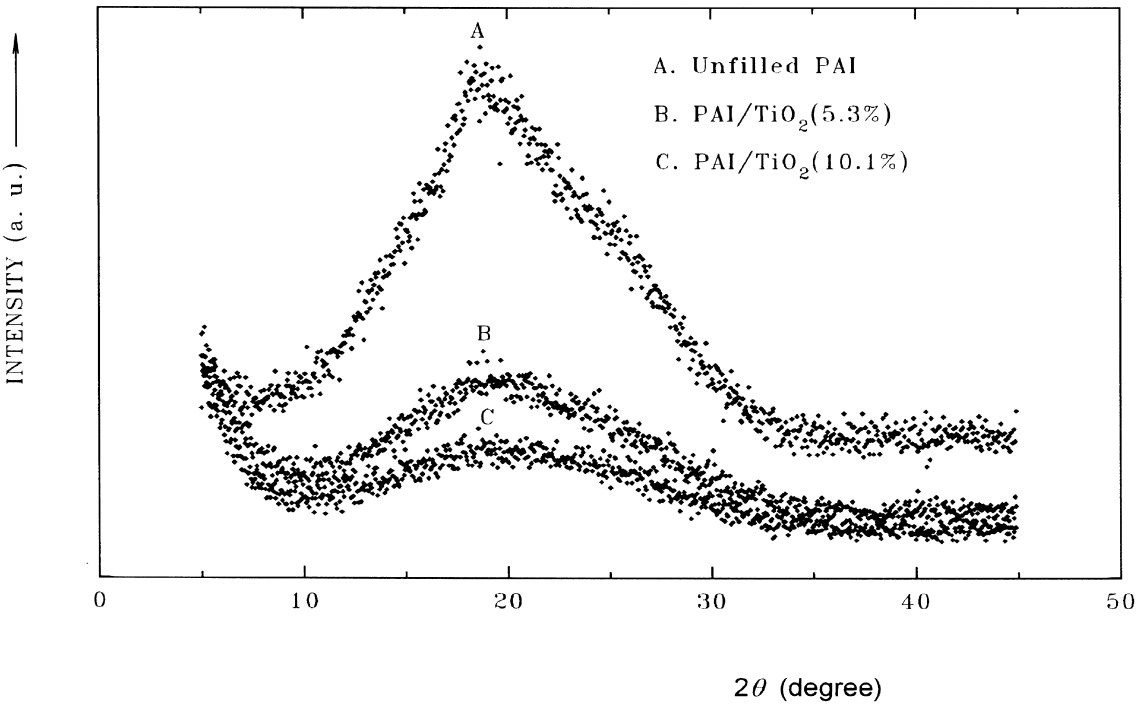


Fig. 8. WAXD patterns of the PAI/$TiO_2$ composites and the pure PAI polymer.

the film fabrication process and that the presence of the $TiO_2$ domains actually serves to disrupt this crystallinity in the composite films.

## 4. Conclusions

Nanosized metal oxide rich domains were incorporated within a high-$T_g$ poly(amide–imide) by a sol–gel process. Under low pH conditions, the high degree of mixing of the organic–inorganic system and the formation of the nanosized $TiO_2$ domains was attributed to hydrogen bonding interactions between the amide group in the PAI polymer and the hydroxyl groups on the inorganic oxide. These interactions seem also to be responsible for disrupting the crystallinity of the PAI polymer during the film formation stage. The $TiO_2$ domains also serve as physical cross-links, decreasing the segmental mobility of the PAI chains, which led to changes in the apparent thermo-mechanical properties of the system. Compared to the pure poly(amide–imide), the poly(amide–imide)/$TiO_2$ composites exhibited higher glass transition temperatures and higher, flattened rubbery plateau moduli.

## Acknowledgements

The authors wish to acknowledge the financial support from NSF CTS-9622437 grant for this project. Thanks are also due to Dr. James E. MaCrath for supplying us with the poly(amide-imide) and Professor Garth Wilkes and Dr. Jianye Wen for access to the DMTA, WAXD and TGA equipment. We also would like to thank Prof. Herve Marand for many valuable discussions.

## References

[1] Brinker CJ, Scherer GW. Sol–gel science: The physics and chemistry of sol–gel processing. San Diego, CA: Academic Press, 1990.
[2] Smaihi M, Jermoumi T, Marigan J, Noble RD. Organic–inorganic gas separation membranes: preparation and characterization. Jour Membrane Sci 1996;116:211–220.
[3] Shrotter JC, Goizet S, Smaihi M, Guizard C. Preparation and characterization of new hybrid organic–inorganic materials for gas separation. Proc Euromembrane (in Bath) 1995;V1:1313–1318.
[4] Wung CJ, Yang Y, Prasad PN, Karasz FE. Poly(*p*-phenylene vinylene)–silica composite: a novel sol–gel processed non-linear optical material for optical waveguides. Polymer 1991;32:604–608.
[5] Krug H, Schmidt H. Organic–inorganic nanocomposites for micro-optical applications. New Jour Chem 1994;18:1125–1134.
[6] Khastgir D, Maiti HS, Bandyopadhyay PC. Polystyrene–titania composite as a dielectric material. Mater Sci Engng 1988;100:245–253.
[7] Wang S, Mark JE. Generation of finely-divided nickel particles in a protective medium an their use as high-activity catalysts. Polym Bull 1992;29:343–348.
[8] Schmidt H, Wolter H. Organically modified ceramics and their applications. Jour Non-Cryst Solids 1990;121:428.
[9] Wang B, Wilkes GL. Novel hybrid inorganic–organic abrasion-resistant coatings prepared by a sol–gel process. J Macromol Sci Pure and Appl Chem 1994;A31:249.
[10] Wang B, Huang H, Brennan AB, Wilkes GL. Synthesis and characterization of new alumina containing organic/inorganic hybrid materials. Polym Prep Div Polym Chem ACS 1989;30(2):146.
[11] Wang B, Wilkes GL. New Ti-PTMO and Zr-PTMO ceramic hybrid materials prepared by the sol–gel method: synthesis and characterization. J Polym Sci: Part A; Polym Chem 1991;29:905–909.

[12] Huang HH, Orler B, Wilkes GL. Structure–property behavior of new hybrid materials incorporating oligometric species into sol–gel glasses. Macromolecules 1987;20:1322–1330.
[13] Spinu M, Brennan A, Rancourt J, Wilkes GL, McGrath JE. MRS Symp Proc 1990;175:179.
[14] Wang S, Ahmad Z, Mark JE. Polym Bull 1993;31:323.
[15] Wang S, Ahmad Z, Mark JE. Macromol Reports 1994;A31 suppl. 3/4:411.
[16] Wang S, Ahmad Z, Mark JE. Chem Mater 1994;6:943.
[17] Morikawa A, Iyoku Y, Kakimoto M, Imal Y. Polym Jour 1992;24:107.
[18] Mark JM, Jiang CY, Tang MY. Simultaneous curing and filling of elastomers. Macromolecules 1984;17:2613–2616.
[19] Mark JE, Pan SJ. Reinforcement of polydimethylsiloxane networks by in situ precipitation of silica: a new method for preparation of filled elastomers. Makromol Chem Rapid Commun 1982;3:681–685.
[20] Landry CJT, Coltrain BK, Brady BK. In situ polymerization of tetraethoxysilane in poly(methyl methacrylate); morphology and dynamic mechanical properties. Polymer 1992;33:1486.
[21] Fitzgerald JJ, Landry CJT, Pochan JM. Dynamic studies of molecular relaxations and interactions in microcomposites prepared by in situ polymerization of silicon-alkoxides. Macromolecules 1992;25:3715–3722.
[22] Nandi M, Conklin JA, Salvati Jr. L, Sen A. Molecular level ceramic/polymer composites. 2. Synthesis of polymer-trapped silica and titania nanoclusters. Chem Mater 1991;3:201.
[23] Saegusa T. Organic polymer–silica gel hybrid; a precursor of highly porous silica gel. J Macromol Sci – Chem 1991;A28(9):817–829.
[24] Mascia L, Kioul A. Jour Mater Sci Lett 1994;13:641.
[25] Iyoku Y, Kakimoto M, Imai Y. High Perform. Polym 1994;6:43.
[26] Goizet S, Schrotter JC, Smaihi M, Deratani A. New Jour Chem 1997;21:461.
[27] Orgaz-Orgaz F. Gel to glass conversion; densification kinetics and controlling mechanism. Jour Non-Cryst Solids 1998;100:115–141.
[28] Livage J, Henry M, Sanchez C. Sol–gel chemistry of transition metal oxides. Prog Solid State Chem 1988;18:259.
[29] Fritsch D, Peinemann KV. Novel highly permselective 6F-poly(amide–imide)s as membrane host for nanosized catalysts. Jour Membrane Sci 1995;99:29–38.
[30] V.N. Sekharipuram, Synthesis and characterization of soluble, melt-processible poly(amide–imide), Ph.D. Thesis, Virginia Polytechnic Institute and State University, 1994.
[31] Moaddeb M, Koros WJ. Jour Membrane Sci 1997;125:143.
[32] Q. Hu, Fabrication and characterization of poly(amide–imide)/$TiO_2$ nanocomposite gas separation membranes Ph.D. Thesis, Virginia Polytechnic Institute and State University, 1997.
[33] Sawyer LC, Grubb DT. Polymer microscopy. London: Chapman and Hall, 1987.
[34] Lopez T, Sanchez E, Bosch P, Meas Y, Gomez R. Mater Chem Phys 1992;32:141.
[35] Nyquist RA, Kagel RO. Infrared spectra of inorganic compounds. New York: Academic Press, 1971 p. 214.
[36] Alpert NL, Kaiser WE, Szymanski HA. IR – theory and practice of infrared spectroscopy. New York: Plenum, 1973.
[37] Bellamy LJ. Advances in infrared group frequencies. London: Methuen, 1968 p. 241.
[38] R.V. Siriwardane, Surface characterization of titanium dioxide, titanium and titanium 6% Al–4% V powders, interaction with water, hydrogen chloride and polymers, Ph.D. Thesis, Virginia Polytechnic Institute and State University, 1981.
[39] Ferry JD. Viscoeleastic properties of polymers. New York: Wiley, 1980.
[40] Nakatta S, Kakimoto M, Imai Y. Polym Jour 1993;25(6):567.